Electrodeposited bismuth monolayers on Au(111) electrodes: Comparison of surface X-ray scattering, scanning tunneling microscopy, and atomic force microscopy lattice structures

5 AUTHORS, INCLUDING:

Chun-hsien Chen
National Taiwan University
97 PUBLICATIONS **3,303** CITATIONS

Andrew A Gewirth
University of Illinois, Urbana-Champaign
207 PUBLICATIONS **5,576** CITATIONS

Jia Wang
Brookhaven National Laboratory
106 PUBLICATIONS **4,811** CITATIONS

Electrodeposited Bismuth Monolayers on Au(111) Electrodes: Comparison of Surface X–ray Scattering, Scanning Tunneling Microscopy, and Atomic Force Microscopy Lattice Structures

Chun-hsien Chen, Keith D. Kepler, and Andrew A. Gewirth*

Department of Chemistry, University of Illinois, 505 S. Mathews Avenue, Urbana, Illinois 61801

B. M. Ocko* and Jia Wang

Department of Physics, Brookhaven National Laboratory, Upton, New York 11973

*Received: December 9, 1992; In Final Form: April 27, 1993*

Surface X-ray scattering (SXS) and scanning tunneling microscope (STM) studies have been carried out to determine the structure of electrochemically deposited Bi monolayers on a Au(111) electrode. Between 10 and 190 mV (relative to bulk deposition), a uniaxially commensurate rectangular phase is formed in which the Bi coverage decreases from 0.646 to 0.616 relative to a gold monolayer. A 25% coverage (2×2) phase is stable between 200 and 280 mV. The structures determined by SXS and STM are in agreement with those determined previously by AFM.

1. Introduction

Atomic force microscopy (AFM),[1] scanning tunneling microscopy (STM),[2] and surface X-ray scattering (SXS)[3] are rapidly becoming important tools for in situ studies of electrode surfaces. Significant insights into electrochemical processes have already been obtained. The STM and AFM techniques provide real space images of the local atomic structure, whereas SXS, a non-probe-based technique with a lateral resolution better than 10^{-3} nm, gives a Fourier transformed image of the atomic structure, averaged over macroscopic regions.

We have previously utilized AFM to show that two distinct underpotentially deposited[4] (upd) Bi adlattice structures exist on the Au(111) electrode surface in acid solution.[5] In Figure 1a, we show the real space structures on the Au(111) surface. The first Bi adlattice structure, existing between 250 and 190 mV vs. $E_{Bi^{3+/0}}$, appears as a commensurate 2×2 adlattice (Figure 1a, middle) exhibiting a 25% coverage. The second adlattice, found between 190 mV and the bulk deposition region (190 mV vs NHE in 0.1 M HClO$_4$), is best described by a rectangular-uniaxially incommensurate $(p \times \sqrt{3})$ structure (Figure 1a, right). For this structure there are two Bi atoms in the cell defined by the orthogonal vectors U_1 and U_2. Whereas $|U_1| = a\sqrt{3}$ ($a = 0.2885$ nm is the Au–Au spacing on the Au(111) surface) is commensurate with the gold lattice, $|U_2|$ depends on potential and is incommensurate with the underlying Au. A similar structure has been reported for Bi on Ag(111).[6] The Bi on Au(111) system is interesting not only because of its unique catalytic behavior[7] but also because it exhibits a phase transition between the open adlattice structure and the more densely packed uniaxially commensurate monolayer.

One of the concerns about information derived from AFM measurement arises from the poor understanding to date of the AFM imaging mechanism. In particular, calculations suggest that pressure exerted by the tip may deform the sample surface,[8] cause material transfer to the tip, and generate images which represent a Fourier synthesis deriving from the tip-sample interactions rather than the real surface. This last point is important with respect to our observation of open metal monolayer surface structures for Bi on Au(111), and in other upd systems.[9] These structures, which are without precedent in the ultra high vacuum (UHV) environment, appear to be stabilized by interactions with anions and/or by partial charge retained on the adatom. It is extremely important to ascertain whether or not the AFM images represent real adatom surface structure.

(a)

Au(111)   (2 × 2)-Bi   (p × √3)-Bi

(b)
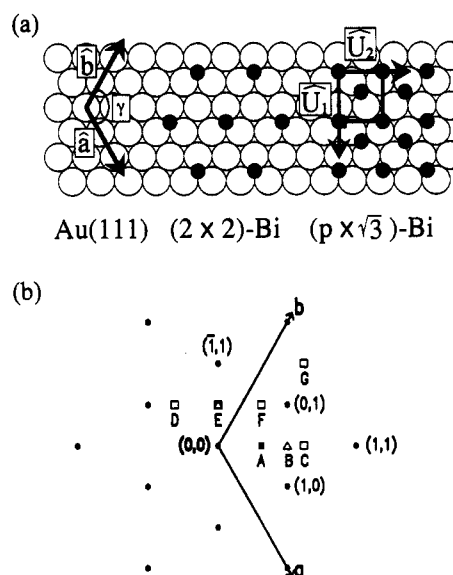
Figure 1. (a) Left: Real space structure of the Au(111) surface. The real space coordinate system on the surface is defined by the vectors **a** and **b** where $|a| = |b| = 2.885$ Å and $\gamma = 120°$. Center: the (2×2)-Bi adlayer structure. Right: (p×√3)-Bi adlayer structure on the Au(111) surface. U_1 and U_2 define the nonprimitive unit cell of the (p×√3) overlayer. The $\langle \bar{1} \, 1 \rangle$ direction is along U_1 while the $\langle 1 \, 1 \rangle$ direction is along U_2. The relationship between the adlayer phases and the underlying gold layers has not been inferred from the present data set. (b) Diffraction pattern for the Au(111) surface projected onto the surface plane. The dark circles correspond to the diffraction pattern from the gold surface without adsorbates. In the (2×2)-Bi adlayer phase, additional diffraction spots are observed at $(\overline{1/2}, 1/2)$ and $(1/2, 1/2)$ as shown by the triangles at E and B, respectively. The observed diffraction pattern in the rectangular (p×√3) phase is shown by the open squares at C $(2\delta, 2\delta)$, D $(1/2 - \delta, 1/2 - \delta)$, E $(\overline{1/2}, 1/2)$, F $(1/2 + \delta, 1/2 + \delta)$, and G $(\bar{1} + 2\delta, 1 + 2\delta)$. No diffraction is observed at A (δ, δ) which indicates that the unit cell is centered along the $\langle 1 \, 1 \rangle$ direction.

In this report, we utilize SXS and STM to evaluate the Bi upd adlattice structures and compare them with those obtained by using AFM. The scattering mechanism of SXS is well established and is based on the Thomson cross section of the electron.[10a] SXS has been applied to surfaces in vacuum[10b] and more recently to in situ electrochemical surface studies.[3] The imaging mechanism of the STM is reasonably well understood in UHV environments,[11] and the use of this technique has been extended to the electrified solid–liquid interface by several groups.[2]

2. Experimental Section

Solution were prepared from reagent grade Bi_2O_3 (Aldrich), ultrapure $HClO_4$, and purified water (Millipore-Q, Millipore Inc.). The solutions contained 1 mM Bi^{3+} and 0.1 M $HClO_4$, and were deoxygenated with either Ar or nitrogen prior to use. All of the potentials reported in this paper are relative to the onset of bulk Bi deposition which is 190 ± 5 mV vs NHE in 0.1 M $HClO_4$.

The X-ray scattering measurements reported in this paper were carried out with focused, monochromatic (λ = 1.54 Å) synchrotron radiation at the National Synchrotron Light Source beam line X22B at Brookhaven National Laboratory. Data is presented after subtraction of the diffuse background scattering which was obtained at 400 mV where no Bi is adsorbed. All of the diffraction data was acquired in reciprocal space using a hexagonal coordinate system (see Figure 1b). The three-dimensional reciprocal space position is denoted by the vector (H,K,L) where the momentum transfer is $(a^*,b^*,c^*) \cdot (H,K,L)$. As shown in Figure 1, there is a 30° rotation between the real space direction along **a** and the reciprocal space direction (1,0). Likewise, there is a 30° rotation between the real space direction along **b** and the reciprocal space direction (0,1). For the Au(111) hexagonal lattice $a^* = b^* = (4\pi/\sqrt{3}a) = 2.52$ Å^{-1}, and $c^* = (2\pi/\sqrt{6}a) = 0.89$ Å^{-1}. The transformation between the hexagonal and the cubic coordinates is given in ref 12. For convenience, we will refer to the reciprocal space position by the surface vector (H,K) since L was fixed at 0.2 for all of the measurements. This corresponds to a grazing angle of 1.25°. A full description of the electrochemical SXS technique, including the single crystal preparation, is presented elsewhere.[12]

STM measurements were carred out using a Nanoscope II STM (Digital Instruments, Santa Barbara, CA) which was calibrated by imaging Au(111) in air. A tungsten rod was etched in 1 M KOH to form the tunneling tip and coated with nail polish (Wet'n Wild no. 401) to insulate from the faradaic background. Reference and counter electrodes were formed from Pt and Au wires, respectively. While the Pt wire is not a true reference, the bulk Bi deposition potential exhibited only ca. 30 mV drift during the 2-h course of the experiment. The tip was maintained at a potential of –500 mV vs the Pt wire reference in order to minimize the faradaic background. Thus the potential between tip and sample varied depending on the potential of working electrode. The Au(111) working electrode was formed by evaporating 120 nm of Au onto V2 grade mica.

3. Results

Figure 2 shows the cyclic voltammetry (CV) on Au(111) obtained in an STM cell at a scan rate of 20 mV/s. The voltammetry was essentially identical with that found in the AFM cell. This CV exhibits two sharp peaks in both the adsorption and stripping processes and agrees well with previous studies.[7] The potentials of the deposition peaks are at 212 and 171 mV whereas the stripping peaks are at 249 and 183 mV. The CV exhibited no changes even after holding the potential in the upd region for more than four hours.

3.1. SXS Measurements. In Figure 3a we display the diffracted intensity obtained at 240 mV after an excursion to 100 mV. Along the $\langle 1\ 1 \rangle$ direction, a single resolution-limited peak is observed exactly at (1/2, 1/2) as shown in Figure 3a. This corresponds to position B in Figure 1b. At this potential we also observe sharp diffraction peaks at $(\overline{1/2}, 1/2)$ (corresponding to E in Figure 1b) as shown in the inset to the figure. Additional peaks are observed at (0, 1/2), at (1/2, 0), and at $(\overline{1/2}, 1)$. On the basis of all of the observed half-order reflections, we conclude that the unit cell is a primitive 2×2 structure, i.e., one Bi atom for every four underlying gold atoms as shown in the middle of Figure 1a. In this potential region, the AFM images also showed a primitive (2×2)-Bi adlayer[5] and the SXS measurement is in complete agreement with this structure.
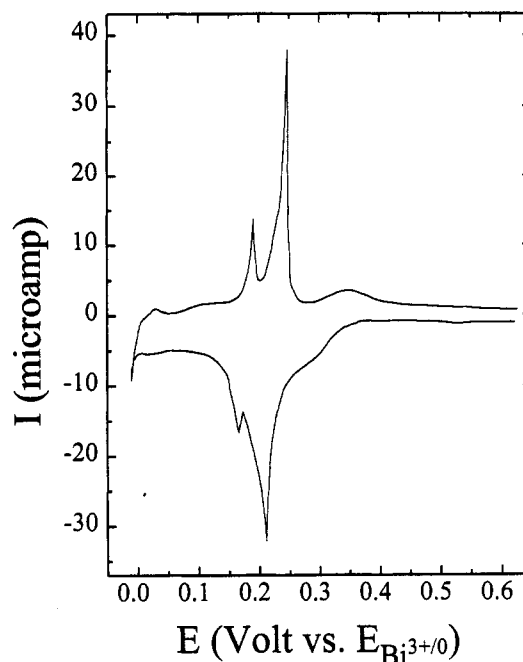

Figure 2. Cyclic voltammogram of Bi electrodeposition on Au(111) obtained in 1 mM Bi^{3+} + 0.1 M $HClO_4$. The scan rate was 20 mV/s.
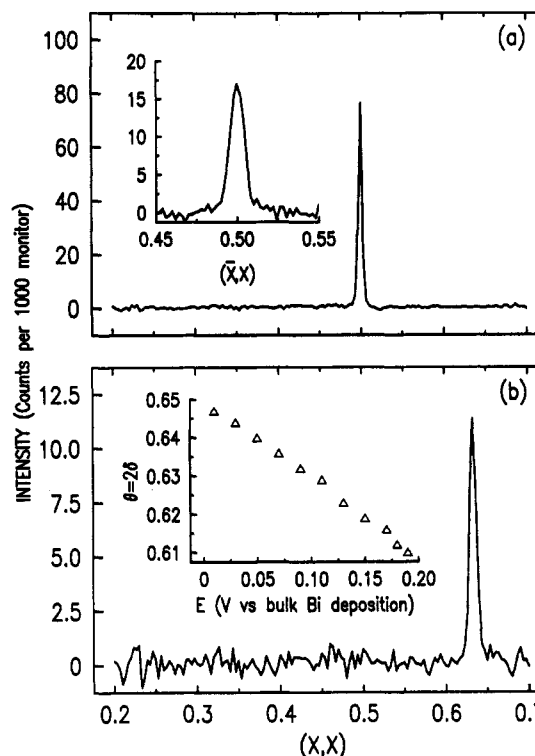

Figure 3. X-ray scattering profiles along the $\langle 1\ 1 \rangle$ direction in reciprocal space after background subtraction. The background data was taken at 400 mV. (a) At 240 mV we observe a sharp diffraction peak at (1/2, 1/2). We also observe a diffraction peak at $(\overline{1/2}, 1/2)$ as shown by the inset. This leads us to conclude that the unit cell is (2×2). (b) At 100 mV we observe a sharp diffraction peak at $(2\delta, 2\delta)$ where 2δ = 0.634 which is incommensurate with the Au(111) lattice. As discussed in the text, this peak and the other diffraction features shown in Figure 1b provides the $(p \times \sqrt{3})$ unit cell assignment. In the inset we plot the coverage, $\theta = 2\delta = p^{-1}$ obtained by measuring the peak position $(2\delta, 2\delta)$ versus the applied potential.

When the potential is moved to 100 mV, a completely different set of diffraction spots is observed. In Figure 3b we display the diffracted intensity at 100 mV along the $\langle 1\ 1 \rangle$ direction after background subtraction. Since the diffraction peak at (1/2, 1/2) is absent, the commensurate 2×2 adlattice which was found at
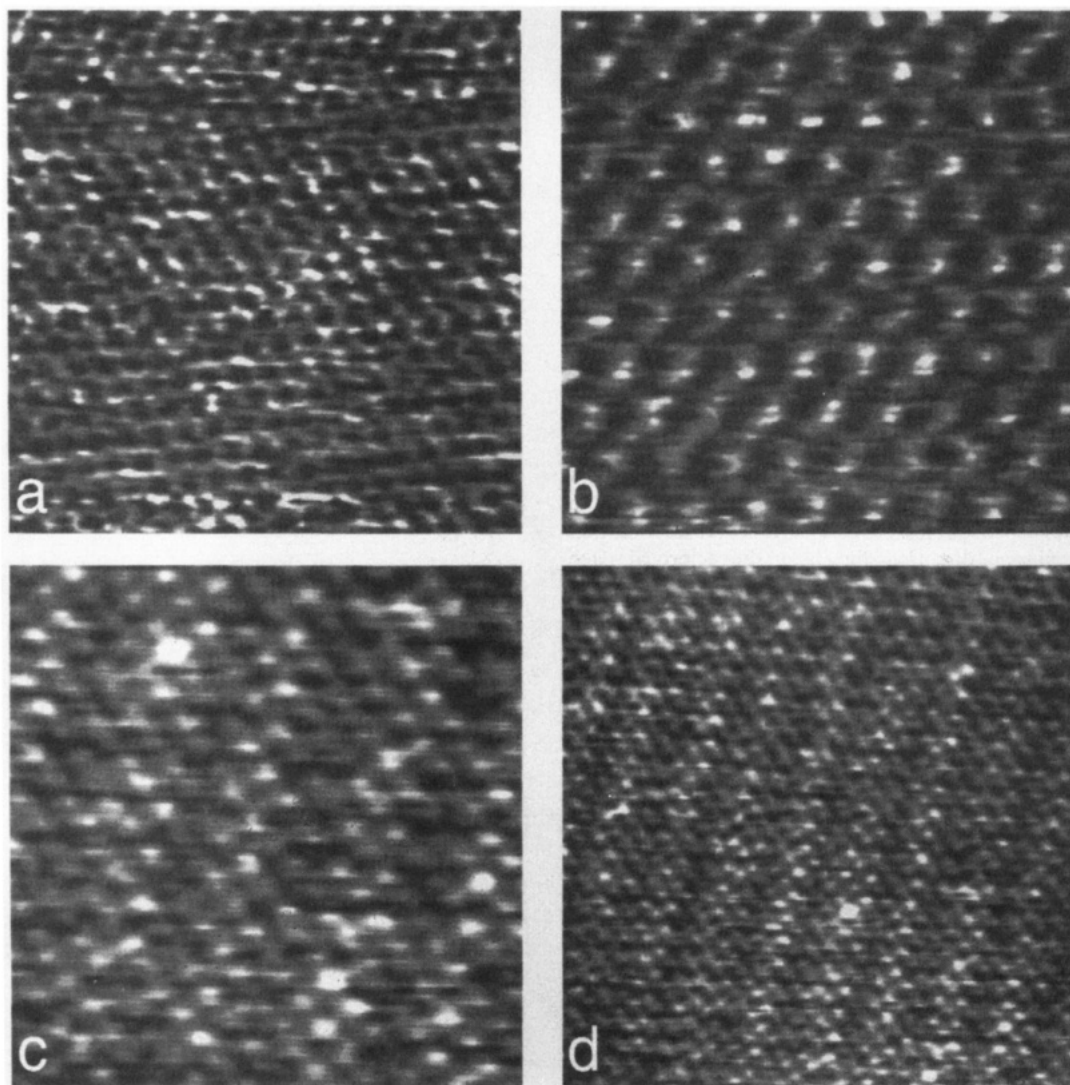
Figure 4. Unfiltered STM images of Bi upd on Au(111). (a) 5×5 nm image of Au(111) obtained at 510 mV. $E_{bias} = -530$ mV; $i_{tip} = 3.5$ nA. (b) 5×5 nm image of the (2×2)-Bi monolayer on Au(111) obtained at 220 mV. $E_{bias} = -165$ mV; $i_{tip} = 4.0$ nA. (c) 5×5 nm STM image of the uniaxially commensurate monolayer of Bi on Au(111) obtained at 100 mV. $E_{bias} = -96$ mV; $i_{tip} = 3.0$ nA. (d) 10×10 nm STM image of the uniaxially commensurate Bi monolayer on Au(111). The Moiré pattern arising from interference between the Bi and Au is clearly seen and the stripes propagate along the U_2 vector shown in Figure 1a.

240 mV has vanished at 100 mV. However, along this same direction in reciprocal space, diffraction is observed at ($2\delta, 2\delta$) with $2\delta = 0.634$. The inset to Figure 3b shows that 2δ varies with potential which implies that the real space structure must be incommensurate with the underlying Au(111) lattice. Diffraction peaks are also observed at ($\overline{1/2} - \delta, 1/2 - \delta$), ($\overline{1/2}, 1/2$), ($\overline{1/2} + \delta, 1/2 + \delta$), and ($\overline{1} + 2\delta, 1 + 2\delta$) as is indicated in Figure 1b. At ($\overline{1/2}, 1/2$) (E in Figure 1b) the diffracted intensity is about a factor of 3 weaker than in the 2×2 phase. The most intense reflections are observed at ($\overline{1/2} - \delta, 1/2 - \delta$) and ($\overline{1/2} + \delta, 1/2 + \delta$) and the second most intense reflection is at ($2\delta, 2\delta$). No diffraction is observed at (δ, δ). Although there are three symmetric directions (rotated from each other by 120°) on the Au(111) surface, for visual simplicity diffraction from only one of these is shown in Figure 1b.

The observed diffraction at 100 mV shown in Figure 1b indicates that the structure of Bi on Au(111) is the rectangular ($p \times \sqrt{3}$) phase shown on the right of Figure 1a. Diffraction at ($2\delta, 2\delta$) implies there are rows of atoms which are separated by a distance $|U_2| = ap = a/(2\delta)$. This relationship defines the dimensionless unit cell length, p, in terms of 2δ which in turn depends on potential. The second Bi atom in the unit cell appears to be well centered along the U_2 direction since diffraction at (δ, δ) is not observed. Diffraction at the positions ($\overline{1/2} + n\delta, 1/2 + n\delta$), where n is

an integer, implies that there is a Fourier component of the electron density wave with a periodicity of $a\sqrt{3}$. This periodicity corresponds to two rows of atoms and is given by the vector U_1 as shown in Figure 1a. The diffraction pattern closely resembles that expected for a centered rectangular phase where the absence of every other diffraction spot implies that there are two atoms per unit cell. However, at some of the positions where the structure factor should vanish for this centered-rectangular cell we observe weak diffraction. If the second Bi atom in the unit cell is accurately centered along the U_1 direction, then the diffraction peak at ($\overline{1/2}, 1/2$) would vanish. This is not the case and implies that the Bi rows must be paired. Toney and co-workers have reached a similar conclusion for Bi on Ag(111).[6] The designation of the ($p \times \sqrt{3}$) rectangular unit cell is consistent with previously reported AFM images[5] and with STM images described in the next section. In addition, the unit cell repeat length $pa = |U_2| = 0.456$ nm compares well with the 0.46 ± 0.04 nm spacing deduced from AFM images.

In the inset to the Figure 3b we show that 2δ, measured in the positive sweep, decreases linearly with potential. Diffraction data was acquired along the $\langle 1\ 1 \rangle$ direction every 20 mV (in both sweep directions) in order to measure 2δ which is given by the center of the diffraction peak. The atomic coverage of Bi can be measured very accurately from the diffraction peaks since the
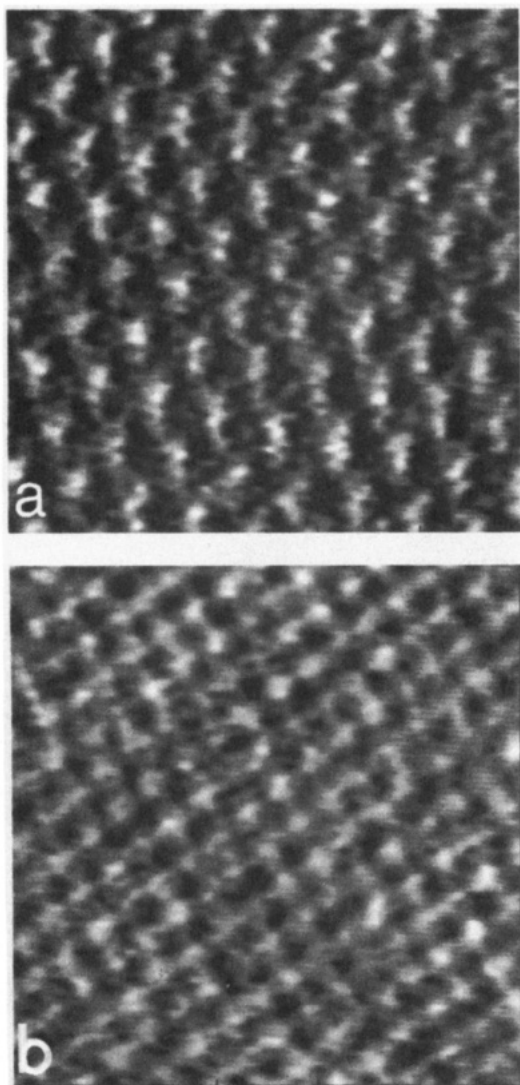
Figure 5. (a) Unfiltered 5 × 5 nm AFM image obtained at 200 mV vs. $E_{Bi^{3+}/0}$ of the (2×2) hexagonal Bi adlattice on Au(111). (b) Unfiltered 5 × 5 nm AFM image at 100 mV of the $(p\times\sqrt{3})$ rectangular Bi adlattice on Au(111).

coverage θ, relative to the underlying gold density, is equal to 2δ. In the negative sweep, the $(p\times\sqrt{3})$ phase is first observed with $2\delta = 0.612$ at 190 mV and the peak position decreases to $2\delta = 0.646$ at 10 mV. This corresponds to a decrease in the magnitude of U_2 from 0.471 to 0.447 nm.

3.2. STM Measurements. At 500 mV, positive of the first deposition peak in the CV shown in Figure 1, atomic resolution images reveal a hexagonal lattice with an atom-atom spacing of 0.29 ± 0.02 nm shown in Figure 4a. We associate this structure with the expected Au(111) lattice which should be observed at this potential. The reconstructed Au(111) lattice should not be observed at +500 mV since this potential is positive of the potential of zero charge (pzc).[12]

Cycling to potentials between 250 and 190 mV gives rise to the (2×2)-Bi adlattice (0.57-nm atom-atom spacing) which is clearly seen in Figure 4b. The atomic arrangement observed in this STM image is essentially identical to the corresponding arrangement in the AFM image shown in Figure 5a. While stable images could be obtained with tunneling currents as low as 1 nA, the best images were obtained between 3 and 4 nA.

Cycling to between 170 and 0 mV gives rise to the uniaxially commensurate Bi adlattice (Figure 4c) exhibiting a 0.34 ± 0.02 nm atom-atom spacing (0.46 ± 0.03 nm spacing along U_2) which is identical to that seen by AFM in Figure 5b. Thus, there is essentially no significant difference in spacing or orientation

between AFM, STM, and SXS results for this system. However, long-range scans of the Bi-covered Au(111) surface reveal an apparent 0.02 ± 0.01 nm modulation in height which propagates in the direction corresponding to U_2 shown on the right in Figure 1a. This Moiré pattern arises from the mismatch between the Bi overlayer and the underlying Au.[13] That the height modulation is seen in only one direction is strong evidence that the monolayer is incommensurate in only one lattice orientation, in agreement with the SXS measurements. The apparent 0.02 ± 0.01 nm average height modulation represents the difference in height between Bi adatoms in or near atop sites on the Au surface and those that are in or near threefold hollow sites. The period of the height modulation along U_2 is every four or five Bi atoms which is entirely consistent with the 0.46-nm Bi–Bi spacing found using SXS in this direction. Analysis of this pattern could provide high-resolution information about the degree of mismatch between the Bi and Au. An analysis of this type has already been undertaken for Pb monolayers on Ag(111).[14] Finally, while the repeat distance spacing found with the STM should be potential dependent (as it was with SXS), drift in our Pt quasi-reference electrode precluded determination of this change.

4. Discussion

The structures provided by the SXS and STM measurements reported above are essentially identical with those we found previously by AFM. AFM images of the (2×2)-Bi and rectangular $(p\times\sqrt{3})$ phases are shown in Figure 5 for completeness. This correspondence of results allows us to proceed with renewed confidence in the AFM measurement. These results are particularly significant because two different structural types are represented in this system: the 2×2 lattice is hexagonal while the uniaxially commensurate monolayer is rectangular. That the AFM can image both correctly, in the same experiment, provides strong evidence that the AFM images are not representative of a multicomponent Fourier synthesis deriving from anomalous interactions between sample and tip. The AFM images are truly representative of the structures occurring on the electrode surface.

In addition to confirming the AFM results, the SXS measurements provides a much better spatial determination of the Bi monolayer. While the AFM determination of the 2×2 adlattice is aided by the inherent lattice symmetry, the absence of a commensurate structure in the rectangular phase makes this task more difficult. In the SXS experiment we have measured the incommensurate lattice constant and the subsequent two-dimensional compressibility. Here the magnitude of U_2 changed from 0.471 to 0.447 nm. This spacing change is well below the AFM resolution limit and subsumed in the average spacing we observe of 0.46 ± 0.03 nm. Whereas the SXS measurement shows that the rectangular $(p\times\sqrt{3})$ structure is not accurately centered, this structural detail cannot be ascertained by either the STM or the AFM. We note, however, that prior solution of the structure at low resolution by AFM simplified the search process during the SXS experiment which can be difficult due to the inherent high resolution.

The lattice constants of gold and silver only differ by 0.25% and one might expect similar behavior for Bi deposition on these two substrates. Indeed, the results of this study in the $(p\times\sqrt{3})$ phase are in reasonable agreement with a study by Toney and co-workers for Bi on Ag(111).[6] First, we note that the most compressed incommensurate lattice constant for Bi equals 0.448 ± 0.001 nm on both (111) surfaces. This suggests that the formation of bulk Bi occurs at the same critical coverage in both cases. Second, the two-dimensional isothermal compressibility (κ_{2D}) for Bi on Au(111), measured from the slope of the lattice constant with potential, equals 1.15 ± 0.05 Å^2/eV which is larger than the value of 0.79 Å^2/eV obtained for Bi on Ag(111). This is consistent with expected differences between Ag and Au systems.[15] Finally, only one current peak is observed in the upd

voltammetry for Bi on Ag(111). The absence of the second peak in the Ag(111) system, observed at the Au(111) electrode (see Figure 2), is consistent with only a uniaxially commensurate-rectangular phase, i.e., no (2×2)-Bi structure.

We have utilized the three emerging *in situ* techniques which provide direct structural information at the solid–liquid interface. The congruence of all three measurements allows us to proceed* with further characterization of electrochemically formed monolayer and multilayer structures.

References and Notes

(1) Manne, S.; Hansma, P. K.; Massie, J.; Elings, V. B.; Gewirth, A. A. *Science* **1991**, *251*, 183–186.

(2) For example (a) Magnussen, O. M.; Hotlos, J.; Nicols, R. J.; Behm, R. J.; Kolb, D. M. *Phys. Rev. Lett.* **1990**, *64*, 2929–2932. (b) Gao, X.; Hamelin, A.; Weaver, M. J. *Phys. Rev. Lett.* **1991**, *67*, 618–621. (c) Hachiya, T.; Honbo, H.; Itaya, K. *J. Electroanal. Chem.* **1991**, *315*, 275. (d) Tao, N. J.; Lindsay, S. M. *Surf. Sci. Lett.* **1992**, *247*, L546–553. (e) Green, M. P.; Hanson, K. J. *Surf. Sci.* **1992**, *259*, L743–749. (f) Oppenheim, I. C.; Trevor, D. J.; Chidsey, C. E. D.; Trevor, P. L.; Sieradzki, K. *Science* **1991**, *254*, 687–689.

(3) For example (a) Ocko, B. M.; Wang, J.; Davenport, A.; Isaacs, H. *Phys. Rev. Lett.* **1990**, *65*, 1466–1469. (b) Melroy, O. R.; Toney, M. F.; Borges, G. L.; Samant, M. G.; Kortright, J. B.; Ross, P. N.; Blum, L. *Phys. Rev. B* **1988**, *38*, 10962–10965.

(4) Kolb, D. M. In *Advances in Electrochemistry and Electrochemical Engineering*; Gerischer, H., Tobias, C. W., Eds.; Wiley; New York, 1978; Vol. 11, pp 125–271.

(5) Chen, C.-h.; Gewirth, A. A. *J. Am. Chem. Soc.* **1992**, *114*, 5439–5440.

(6) Toney, M. F.; Gordon, J. G.; Samant, M. G.; Borges, G. L.; Wiesler, D. G.; Yee, D.; Sorensen, L. B. *Langmuir* **1991**, *7*, 796–802.

(7) Sayed, S. M.; Juttner, K. *Electrochim. Acta* **1983**, *28*, 1635–1641.

(8) Landman, U.; Luedtke, W. D.; Burnham, N. A.; Colton, R. J. *Science* **1990**, *248*, 454–461.

(9) (a) Chen, C.-h.; Vesecky, S. M.; Gewirth, A. A. *J. Am. Chem. Soc.* **1992**, *114*, 451–458. (b) Chen, C.-h.; Gewirth, A. A. *Phys. Rev. Lett.* **1992**, *68*, 1571–1574.

(10) (a) Warren, B. E. *X-ray Diffraction*; Addison-Wesley: Boston, MA, 1969. (b) Robinson, I. K. In *Handbook on Synchrotron Radiation*; Brown, G., Moncton, D. E., Eds.; Elsevier Science: New York; 1991; Vol. 3, pp 221–266.

(11) Chen, C. J. *Introduction to Scanning Tunneling Microscopy*; Oxford University Press: New York, 1993.

(12) Wang, J.; Ocko, B. M.; Davenport, A.; Isaacs, H. S. *Phys. Rev. B* **1992**, *46*, 10321–10338.

(13) The STM imaging area (25 nm²) is small relative to the average domain size (ca. 1×10^6 nm²) on the Au(111) surface. Thus only one domain contributes to the Moiré pattern, and only one orientation of the $(p\times\sqrt{3})$ phase is observed.

(14) Muller, U.; Carnal, D.; Siegenthaler, H.; Schmidt, E.; Loranz, W. J.; Obretenov, W.; Schmidt, U.; Staikov, G.; Budevski, E. *Phys. Rev. B*, **1992**, *46*, 12899–12901.

(15) Toney, M. F.; Melroy, O. R.; Gordon, J. G. *Soc. Photoopt. Inst. Eng.* **1991**, *1550*, 1.